

## Article

# Toward the Estimation of All-Weather Daytime Downward Longwave Radiation over the Tibetan Plateau

Zhiyong Long <sup>1,\*</sup>, Lirong Ding <sup>2</sup>, Ji Zhou <sup>2</sup>  and Tianhao Zhou <sup>2</sup><sup>1</sup> College of Meteorology and Oceanography, National University of Defense Technology, Changsha 410073, China<sup>2</sup> School of Resources and Environment, University of Electronic Science and Technology of China, Chengdu 611731, China; dlryouxiang@163.com (L.D.); jzhou233@uestc.edu.cn (J.Z.); zhoutianhao1827@163.com (T.Z.)

\* Correspondence: longzhiyong17@nudt.edu.cn; Tel./Fax: +86-0731-84574064

**Abstract:** Downward longwave radiation (DLR) is a critical parameter for radiation balance, energy budget, and water cycle studies at regional and global scales. Accurate estimation of the all-weather DLR with a high temporal resolution is important for the estimation of the surface net radiation and evapotranspiration. However, most DLR products involve instantaneous DLR estimates based on polar orbiting satellite data under clear-sky conditions. To obtain an in-depth understanding of the performances of different models in the estimation of DLR over the Tibetan Plateau, which is a focus area of climate change study, this study tests eight methods for clear-sky conditions and six methods for cloudy conditions based on ground-measured data. It is found that the Dilley and O'Brien model and the Lhomme model are most suitable for clear-sky conditions and cloudy conditions, respectively. For the Dilley and O'Brien model, the average root mean square error (RMSE) of DLR under clear-sky conditions is approximately 22.5 W/m<sup>2</sup> for nine ground sites; for the Lhomme model, the average RMSE is approximately 23.2 W/m<sup>2</sup>. Based on the estimated cloud fraction and meteorological data provided by the China Land Surface Data Assimilation System (CLDAS), hourly all-weather daytime DLR with a 0.0625° resolution over the Tibetan Plateau is estimated. Results demonstrate that the average RMSE of the estimated hourly all-weather DLR is approximately 26.4 W/m<sup>2</sup>. With the combined all-weather DLR model, the hourly all-weather daytime DLR dataset with a 0.0625° resolution from 2008 to 2016 over the Tibetan Plateau is generated. This dataset can contribute to studies associated with the radiation balance and energy budget, water cycle, and climate change over the Tibetan Plateau.

**Keywords:** downward longwave radiation (DLR); all-weather; Tibetan Plateau

**Citation:** Long, Z.; Ding, L.; Zhou, J.; Zhou, T. Toward the Estimation of All-Weather Daytime Downward Longwave Radiation over the Tibetan Plateau. *Atmosphere* **2021**, *12*, 1692. <https://doi.org/10.3390/atmos12121692>

Academic Editors: Rui Salgado, Maria José Monteiro, Mariana Bernardino, David Carvalho, Flavio T. Couto, Rita M. Cardoso, João P. A. Martins and Joao Carlos Andrade dos Santos

Received: 21 November 2021

Accepted: 9 December 2021

Published: 17 December 2021

**Publisher's Note:** MDPI stays neutral with regard to jurisdictional claims in published maps and institutional affiliations.



**Copyright:** © 2021 by the authors. Licensee MDPI, Basel, Switzerland. This article is an open access article distributed under the terms and conditions of the Creative Commons Attribution (CC BY) license (<https://creativecommons.org/licenses/by/4.0/>).

## 1. Introduction

Downward longwave radiation (DLR) is a critical parameter for radiation balance, energy budget, and water cycle studies at regional and global scales [1]. The estimation of the surface net radiation, which serves the modeling of land surface processes (e.g., surface evapotranspiration estimation and climate change analysis), is directly related to the accuracy of DLR [2]. Thus, accurate estimation of DLR allows a better understanding of land surface processes and climate change.

In the past decades, scientific communities have proposed a series of models to estimate DLR. For example, Ångström [3] developed the first empirical model based on the Stefan-Boltzmann formula. In this study, meteorological parameters were used to calculate the atmospheric water pressure ( $e$ ), and then the relationship between  $e$  and the atmospheric emissivity ( $E_s$ ) was established; thus, DLR was calculated based on  $E_s$  according to the Stefan-Boltzmann formula. Subsequently, Brunt, Brutsaert (1975), Idso, Idso and Jackson, Prata, and Dilley and O'Brien [4–9] have successively proposed several empirical models for estimating  $E_s$  through meteorological parameters for clear-sky conditions. In contrast,

Swinbank [10] proposed an empirical method to estimate DLR directly using only the surface air temperature ( $T_a$ ) for clear-sky conditions.

The aforementioned empirical models are only applicable for clear-sky conditions because the influences of clouds on DLR are not addressed. It is generally known that the wavelength range for longwave radiation is 4.0–100.0  $\mu\text{m}$ , and the longwave radiation is mainly affected by  $\text{H}_2\text{O}$ ,  $\text{CO}_2$ , and  $\text{O}_3$  molecules and cloud water droplets [7]. Clouds increase DLR significantly; therefore, it is necessary to consider the influence of clouds in the estimation of DLR. Many studies have tried to estimate DLR affected by clouds. For example, Crawford and Duchon, Jacobs, Konzelmann et al., Lhomme et al., Maykut and Church, and Sugita and Brutsaert [1,11–15] developed a series of cloud correction models to estimate DLR for cloudy conditions.

In order to satisfy different applications, the models for estimating DLR under clear-sky ( $\text{DLR}_0$ ) and DLR cloudy conditions ( $\text{DLR}_C$ ) have been examined and tested in different regions. For example, to better predict the frost caused by the longwave radiation deficit during the planting period in the Andean Plateau, Lhomme et al. (2007) [13] tested seven clear-sky models at two ground stations and corrected the Brutsaert model [5]; furthermore, an empirical model was also developed to estimate DLR under cloudy conditions. Based on ground observations in Florida, Choi et al. (2008) [16] estimated the daily DLR over different land surfaces under both clear-sky and cloudy conditions and then determined the most suitable model for the regions under examination. Wang and Liang [17] used two widely accepted models, the Brunt model [4] and Brutsaert model [5], to estimate global DLR under both clear-sky and cloudy conditions, based on 3200 ground stations from 1973 to 2008; they succeeded in discovering that the daily average DLR increased year by year. Carmona et al. [18] estimated the daytime instantaneous DLR using different clear-sky and cloudy models based on the ground measurements in Tandil in Buenos Aires Province, Argentina, and proposed two multiple linear regression models to estimate DLR under all-weather conditions.

With the development of earth observations, acquisition of multiple satellite remote sensing data sets has become increasingly feasible. Therefore, the estimation of DLR through remote sensing data has become an effective way to obtain spatially dense DLR data. For example, Wang and Liang [19] developed linear and nonlinear models using a hybrid method to directly derive the instantaneous DLR under clear-sky conditions from the 1 km top of atmosphere (TOA) radiance of the Moderate Resolution Imaging Spectroradiometer (MODIS). Yu et al. (2011) [20] used three different algorithms to estimate the clear-sky DLR from MODIS data in the Heihe River Basin, Northwest China. Wu [21] estimated DLR using eight models under clear-sky conditions based on meteorological parameters derived from the MODIS atmospheric profile products (i.e., MOD07\_L2/MYD07\_L2); they further proposed a multimodel ensemble approach to integrate the estimates of the eight models. Yu et al. [22] estimated the clear-sky DLR from the Chinese HJ-1B thermal data, based on extensive radiative transfer simulation and statistical analysis. Wang et al. [23] proposed a model that could improve the accuracy of DLR estimation from satellite data for conditions with heavy dust aerosol levels, and the results demonstrate that the level of dust aerosols has an obvious “warming” effect on DLR, compared with other aerosols. These studies have illustrated that it is feasible to estimate DLR through parametric models, using satellite remote sensing data. Most of these studies are based on polar orbit satellite data. Thus, the obtained DLR is the instantaneous value under clear-sky conditions. How to obtain the all-weather DLR with a high temporal resolution (e.g., hourly) is a key problem that needs resolution.

The Tibetan Plateau, which is known as “the roof of the world” and “the third pole”, is a focus region of radiation balance, energy budget, and climate change studies [24]. DLR is one of the most important parameters for in-depth understanding of the radiation budget process in this area. However, the ground sites providing DLR measurements are very rare, and the acquisition of DLR is very difficult in the Tibetan Plateau. Furthermore, the applicability of the associated parameterization model over the Tibetan Plateau is still

unknown. Therefore, obtaining all-weather DLR products with a high temporal resolution according to the characteristics of the Tibetan Plateau is a problem currently faced by the scientific communities.

Most of the parameterization models for estimating DLR are obtained by model training, based on the ground measured data in different regions. The applicability of these models in different regions varies. Therefore, when using these DLR models, their applicability should be tested first. In this context, the objectives of this study are (i) to test the current models for estimating DLR under both clear-sky and cloudy conditions, based on ground-measured meteorological data and to determine the optimal model(s) suitable for the Tibetan Plateau, and (ii) to estimate the all-weather DLR with a high temporal resolution over the Tibetan Plateau, based on the optimal model(s). This study can compensate for the shortcoming that DLR estimated from remote sensing data has a low temporal resolution under clear-sky conditions. The generated all-weather DLR can contribute to better estimation of the surface net radiation and surface evapotranspiration over the Tibetan Plateau.

## 2. Study Area and Datasets

### 2.1. Study Area

The study area is the Tibetan Plateau (73° E–106° E, 40° N–23° N), which has an extraordinary impact on the climate of the surrounding area and even the world. The digital elevation model (DEM) of the Tibetan Plateau is provided in Figure 1. The study area has an average elevation of over 4000 m a.s.l. In the southeastern part of the mountain area, the elevation varies very sharply. In the northwestern part of the Tibetan Plateau, there are many glaciers, and this area is the birthplace of numerous rivers in Asia. Thus, the Tibetan Plateau is also known as “the Asian water tower” [24,25]. The middle of the Tibetan Plateau has a very high altitude. The complex terrain of the Tibetan Plateau induces a complex atmosphere. Due to the importance of its regional function and the complexity of the natural environment, DLR estimation in the Tibetan Plateau is always a challenging task.

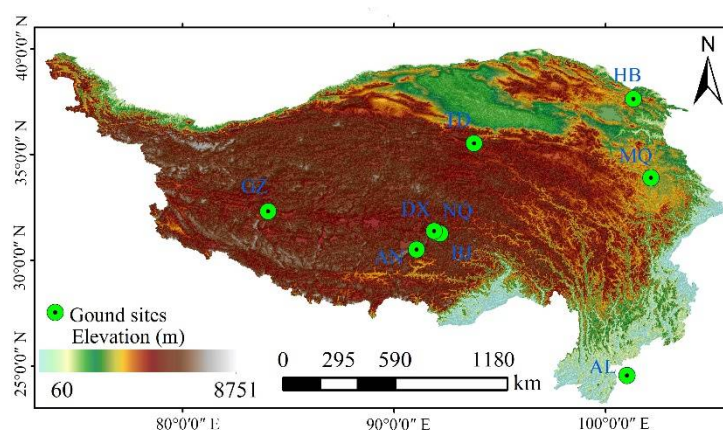


**Figure 1.** Digital elevation model (DEM) of the Tibetan Plateau and the experimental sites that provide the ground measured meteorological data as well as DLR (Note: NQ and BJ are spatially close to each other; thus, these two sites overlap on this map).

### 2.2. Datasets

#### 2.2.1. Ground Measurements

In this study, an observational dataset from nine ground sites is used to examine the performance of associated DLR models over the Tibetan Plateau. The spatial locations of the nine experimental sites are provided in Figure 1, and details of these nine sites are presented in Table 1. These sites provide the instantaneous surface air temperature ( $T_a$ ), relative air humidity ( $RH$ ), ground air pressure ( $q$ ), downward solar radiation (DSR), and DLR. The meteorological observation data (i.e.,  $T_a$ ,  $RH$ ,  $q$ , and DSR) from all sites will be

used to test the applicability of DLR models over the Tibetan Plateau. Among the nine sites, DLR measurements of five sites (i.e., DX, HB, AL, MQ, and NQ) will be used to evaluate the estimated all-weather DLR based on the CLDAS (China Land Surface Data Assimilation System), because only these five sites have measurements during the time span of the CLDAS data. It should be noted that all ground site data is independent of the CLDAS data. Thus, both the test and validation results based on ground-measured data are acceptable [26–28]. For the validity of the model test and the validation of DLR estimation results, the data records with evident observation errors are removed.

**Table 1.** The nine ground sites providing the measurements of  $T_a$ ,  $RH$ ,  $q$ , DSR, and DLR.

Site	Interval (min)	Acquisition Period	Data Source
AN	60	1 October 2002–31 December 2004	CEOP-CAMP <sup>1</sup> ( <a href="https://data.eol.ucar.edu/">https://data.eol.ucar.edu/</a> , accessed on 10 December 2020) [29]
BJ	60	1 October 2002–31 December 2004	CEOP-CAMP <sup>1</sup> ( <a href="https://data.eol.ucar.edu/">https://data.eol.ucar.edu/</a> , accessed on 10 December 2020) [29]
TD	60	1 October 2002–31 December 2004	CEOP-CAMP <sup>1</sup> ( <a href="https://data.eol.ucar.edu/">https://data.eol.ucar.edu/</a> , accessed on 10 December 2020) [29]
GZ	60	1 October 2002–31 December 2004	CEOP-CAMP <sup>1</sup> ( <a href="https://data.eol.ucar.edu/">https://data.eol.ucar.edu/</a> , accessed on 10 December 2020) [29]
DX	30	1 January 2002–31 December 2012	ChinaFLUX <sup>2</sup> ( <a href="http://www.chinaflux.org/">http://www.chinaflux.org/</a> , accessed on 10 December 2020) [30,31]
HB	30	1 January 2010–31 December 2010	ChinaFLUX <sup>2</sup> ( <a href="http://www.chinaflux.org/">http://www.chinaflux.org/</a> , accessed on 10 December 2020) [32]
AL	30	1 January 2012–31 December 2013	ChinaFLUX <sup>2</sup> ( <a href="http://www.chinaflux.org/">http://www.chinaflux.org/</a> , accessed on 10 December 2020) [33]
MQ	30	1 January 2013–31 December 2013	NIEER <sup>3</sup> ( <a href="http://www.nieer.cas.cn/">http://www.nieer.cas.cn/</a> , accessed on 10 December 2020) [34]
NQ	30	1 January 2010–31 December 2010	ChinaFLUX <sup>2</sup> ( <a href="http://www.chinaflux.org/">http://www.chinaflux.org/</a> , accessed on 10 December 2020) [35]

<sup>1</sup> Coordinated Energy and Water Cycle Observation Project (CEOP) Enhanced Observing Periods 3 and 4 (EOP-3 and EOP-4) CEOP Asia-Australia Monsoon Project (CAMP) [29]; <sup>2</sup> China FLUX Observation and Research Network; <sup>3</sup> Northwest Institute of Eco-Environment and Resources Chinese Academy of Sciences [34].

### 2.2.2. Assimilation Dataset

To estimate DLR of the entire Tibetan Plateau, the meteorological data provided by the China Land Surface Data Assimilation System (CLDAS) are used [26–28]. Specifically, the meteorological variables derived from the CLDAS include the air specific humidity (SH),  $T_a$ ,  $q$ , and DSR. The CLDAS data have a spatial resolution of  $0.0625^\circ$  and a temporal resolution of 1 h. The CLDAS combines multiple types of source data. The first type of data are ground observation data, including the hourly air temperature, air pressure, humidity, wind speed, precipitation and other meteorological variables, observed at more than 2400 national-level automatic weather stations and approximately 40,000 regional automatic weather stations in China. The second type of data are the European Center for Medium-Range Weather Forecasts (ECMWF) released data products, with a 3 h temporal resolution and a  $0.125^\circ$  spatial resolution [36–38]. The meteorological variables of the ECMWF are the  $T_a$ , air humidity, wind speed, and ground pressure. The third type of data are the global ozone, atmospheric precipitation, ground pressure, and other data products released by the National Centers for Environmental Prediction (NCEP) [39–41]. The fourth type of data include precipitation products and other meteorological parameters released by the National Satellite Meteorological Center of China. Therefore, compared with similar products, the CLDAS product is believed to have better quality and more reasonable spatial and temporal characteristics of the meteorological variables in China [26,27].

### 2.2.3. Auxiliary Datasets

To estimate the theoretical DSR under clear-sky conditions, the DEM acquired by the Shuttle Radar Topography Mission (SRTM) is also collected in this study. The original resolution of the DEM data is 90 m. To match the DEM and the CLDAS dataset, the spatial resolution of the DEM data is resampled to  $0.0625^\circ$ . In the resampling process, the DEM

of a 0.0625° pixel is obtained by weighted average of the DEM of the all high-resolution pixels within the 0.0625° pixel.

### 3. Methodology

#### 3.1. Clear-Sky Model

In this study, eight widely used empirical DLR models for clear-sky conditions are selected. Details of these eight models are presented in Table 2. These models are tested and evaluated based on meteorological observations provided by the ground sites. Based on the evaluation results of the eight models, the optimal model will be selected to estimate DLR under clear-sky conditions for the Tibetan Plateau. For the eight selected models, the input  $T_a$  (unit: K) is provided by the ground observations or the CLDAS dataset. Thus,  $e$  is the only unknown parameter. It can be calculated according to:

$$e = e_s \times RH \tag{1}$$

where  $e_s$  is the saturation vapor pressure (unit: hpa).

When the surface air temperature is higher than 0 °C,  $e_s$  can be calculated according to [42]:

$$e_s = 6.1078 \exp\left[\frac{17.2693882(T_a - 273.16)}{T_a - 35.86}\right] \tag{2}$$

When the surface air temperature is below 0 °C,  $e_s$  can be calculated as [42]:

$$e_s = 6.112 \exp\left[\frac{17.67t}{t + 243.5}\right] \tag{3}$$

where  $t$  is the surface air temperature in °C and  $e_s$  is the saturation vapor pressure in hpa.

Because RH is not available from the CLDAS dataset, the following formula is employed to calculate  $e$ :

$$e = \frac{q \times SH}{0.622 + 0.378 \times SH} \tag{4}$$

where  $q$  is the ground air pressure (unit: hpa) and  $SH$  is the air specific humidity.

**Table 2.** The eight selected models for estimating DLR ( $DLR_0$ ) under clear-sky conditions.

Abbreviation	Formula	Source
AN-CK	$DLR_0 = \sigma(0.83 - 0.18 \times 10^{-0.067e})T_a^4$	[3]
BT-CK	$DLR_0 = \sigma(0.605 + 0.048e^{0.5})T_a^4$	[4]
SW-CK	$DLR_0 = 5.31 \times 10^{-13}T_a^6$	[10]
IJ-CK	$DLR_0 = \sigma(1 - 0.261 \exp(-0.00077(273 - T_a)^2))T_a^4$	[7]
BR-CK	$DLR_0 = \sigma(1.24(\frac{e}{T_a})^{\frac{1}{2}})T_a^4$	[5]
ID-CK	$DLR_0 = \sigma(0.7 - 5.95 \times 10^{-5}e \exp(\frac{1500}{T_a}))T_a^4$	[6]
PR-CK	$DLR_0 = \sigma(1 - (1 + 46.5eT_a) \exp(-(1.2 + 139.5e/T_a)^{0.5}))T_a^4$	[8]
DO-CK	$DLR_0 = 59.38 + 113.7(\frac{T_a}{273.3}) + 99.96(\frac{93e}{5T_a})^{0.5}$	[9]

Note:  $DLR_0$  is DLR under clear-sky conditions;  $\sigma$  is the Stefan-Boltzmann constant;  $e$  and  $T_a$  are the screen level water vapor pressure and air temperature, respectively.

#### 3.2. Cloudy-Sky Model

When clouds occur, the water content in the atmosphere increases significantly, and so does the atmospheric effective emissivity. According to the Stefan-Boltzmann’s law, an increase in the atmospheric effective emissivity will cause an increase in DLR. Therefore, the estimation of DLR under clear-sky conditions and cloudy conditions is evidently different. How to correctly estimate DLR under cloudy conditions is the most difficult part in DLR estimation. Several models for estimating DLR under cloudy conditions have been proposed by literatures. In this study, six widely used models are selected and tested. Details of these models are presented in Table 3. One should note that these six models were trained in different study areas and they were reported to yield good performance in

their corresponding areas. It is also worth to note that the training area of LH-CL is similar to the Tibetan Plateau.

**Table 3.** The six selected models for estimating DLR under cloudy conditions.

Abbreviation	Formula	Training Area	Source
MC-CL	$DLR_c = DLR_0(1 + 0.22c^{2.75})$	Barrow Alaska	[14]
JA-CL	$DLR_c = DLR_0(1 + 0.26c)$	Broughton Island	[11]
SB-CL	$DLR_c = DLR_0(1 + 0.0496c^{2.45})$	northeastern Kansas	[15]
KO-CL	$DLR_c = DLR_0(1 - c^4) + 0.952c^4\sigma T_a^4$	Greenland Ice Sheet	[12]
CD-CL	$DLR_c = DLR_0(1 - c) + c\sigma T_a^4$	36.61° N, 97.49° W *	[1]
LH-CL	$DLR_c = DLR_0(1.03 + 0.34c)$	Andean Altiplano	[13]

Note:  $DLR_c$  and  $c$  are DLR under cloudy conditions and the cloud fraction, respectively; \* only the latitude and longitude are provided by the reference, without the name of the training area.

Because cloud fraction observations are usually not available, there are no cloud parameters in the ground observation and CLDAS data. Fortunately, the hourly DSR is available in both ground observation and CLDAS data. Thus, we use the following equation to calculate the cloud fraction [1]:

$$c = 1 - \frac{DSR}{DSR_0} \tag{5}$$

where DSR and  $DSR_0$  are the actual downward solar radiation and the theoretical downward solar radiation, respectively.

$DSR_0$  in Equation (5) can be calculated based on the location, time, and altitude; the detailed process is provided in the Appendix A. DSR is derived from the ground measurements. When  $c$  is lower than 0.05, it is assumed that the weather is clear-sky.

### 3.3. Evaluation Metrics

To quantitatively evaluate the test results of the clear-sky and cloudy-sky models and the estimation accuracy of the final all-weather DLR, the mean bias error (MBE) and root mean squared error (RMSE) are used as evaluation metrics. MBE can reflect the overestimation or underestimation, while RMSE can measure the deviation between the estimate and the true value. MBE and RMSE are calculated as follows:

$$MBE = \frac{\sum_{i=1}^N (DLR_e - DLR_{site})}{N} \tag{6}$$

$$RMSE = \sqrt{\frac{\sum_{i=1}^N (DLR_e - DLR_{site})^2}{N}} \tag{7}$$

where  $DLR_e$  and  $DLR_{site}$  are the estimated DLR and the ground measured DLR, respectively, and  $N$  is the sample size.

## 4. Results and Discussion

To test the applicability of every DLR model over the Tibetan Plateau, we use different models to estimate DLR and then validate the DLR estimate against the ground measurements. In the validation, the root mean squared error (RMSE), mean bias error (MBE) and coefficient of determination ( $R^2$ ) of the estimates of the different models are calculated as validation indices. Then, the optimal model(s) will be used to estimate DLR of the entire Tibetan Plateau.

### 4.1. Estimated DLR for the Ground Sites

#### 4.1.1. Under Clear-Sky Conditions

We estimate  $DLR_0$  of each site based on the DLR estimation method for clear-sky conditions, listed in Table 2. We find that the BR-CK model has a large systematic error of up to  $100 \text{ W/m}^2$  for all the nine sites. Thus, the validation results of this model are not

provided here. For the other seven models, the errors are presented in Table 4. The average RMSE is  $22.5 \pm 6.4 \text{ W/m}^2$  for DO-CK. It is clear that this model has higher accuracy and stability than the other six models for most sites.

**Table 4.** Evaluation of the estimated DLR by the seven models under clear-sky conditions for the nine sites.

Method		Site									Average Value
		AL	AN	TD	BJ	DX	GZ	HB	MQ	NQ	
AN-CK	RMSE ( $\text{W/m}^2$ )	16.7	22.8	31.1	30.1	43.4	17.8	29.1	23.7	26.6	26.8
	MBE ( $\text{W/m}^2$ )	10.3	10.4	16.1	20.2	38.4	11.9	5.4	−2.7	−4.7	11.7
	R <sup>2</sup>	0.72	0.73	0.61	0.7	0.84	0.88	0.68	0.75	0.84	0.75
BT-CK	RMSE ( $\text{W/m}^2$ )	13.2	20.9	27.9	25.3	36.3	13.7	29.7	18.3	30.9	24.1
	MBE ( $\text{W/m}^2$ )	−2.9	2.3	7.9	11.7	29.5	3.1	−3.3	−6.4	−13.7	3.1
	R <sup>2</sup>	0.73	0.72	0.64	0.7	0.83	0.88	0.67	0.74	0.84	0.75
SW-CK	RMSE ( $\text{W/m}^2$ )	19.4	28.8	35.1	43.1	52.7	36.6	36.9	22.8	29.5	33.9
	MBE ( $\text{W/m}^2$ )	9.5	13.7	17.1	27.7	45	29.8	3.6	5.3	2.7	17.2
	R <sup>2</sup>	0.61	0.65	0.54	0.54	0.71	0.79	0.5	0.81	0.75	0.66
IJ-CK	RMSE ( $\text{W/m}^2$ )	19.8	37.2	46.0	48.4	62.0	42.1	40.8	26.0	33.8	39.6
	MBE ( $\text{W/m}^2$ )	10.9	28.1	34.5	40	56.1	38.1	18.8	16.4	14.4	28.6
	R <sup>2</sup>	0.61	0.64	0.59	0.56	0.75	0.81	0.49	0.82	0.78	0.67
ID-CK	RMSE ( $\text{W/m}^2$ )	23.2	38.5	37.2	36.7	48.6	26.2	36.6	23.6	35.2	34.1
	MBE ( $\text{W/m}^2$ )	−15.6	13.3	20.2	22.8	38.5	18.3	2.6	−2.7	−4.1	10.4
	R <sup>2</sup>	0.6	0.61	0.56	0.5	0.7	0.79	0.54	0.8	0.73	0.65
PR-CK	RMSE ( $\text{W/m}^2$ )	13.4	24.3	32.7	31.8	44.7	20.1	30.7	24.6	29.0	27.9
	MBE ( $\text{W/m}^2$ )	4.3	11.4	17.6	21.2	38.7	13.8	5.0	−3.4	−4.5	11.6
	R <sup>2</sup>	0.75	0.71	0.61	0.67	0.82	0.86	0.68	0.73	0.82	0.74
DO-CK	RMSE ( $\text{W/m}^2$ )	14.1	19.8	25.1	19.5	29.7	14.8	27.2	19.7	34.3	22.5
	MBE ( $\text{W/m}^2$ )	−6.3	−3.4	1.9	4.6	22.5	−8.3	−6.1	−10.6	−20.8	−2.8
	R <sup>2</sup>	0.77	0.79	0.71	0.78	0.89	0.91	0.77	0.89	0.87	0.82

To further verify the systematic errors of the models, the MBE of each model for each site is also calculated. As presented in Table 4, AN-CK, SW-CK, IJ-CK, ID-CK, and PR-CK clearly overestimated DLR<sub>0</sub>; BT-CK had a slight overestimation; DO-CK had a slight underestimation and had the minimum systematic error: the average MBE and RMSE are  $-2.8 \pm 6.4 \text{ W/m}^2$   $22.5 \text{ W/m}^2$ .

The R<sup>2</sup> values of the evaluations are also provided in Table 4. The R<sup>2</sup> of the DO-CK model is  $0.82 \pm 0.066$ . The other six models all have lower R<sup>2</sup> values than the DO-CK model, and at different sites; the differences between models are large. The main reason for the R<sup>2</sup> difference is that the models used to estimate DLR<sub>0</sub> are empirical models, and they have different applicability in the Tibetan Plateau. After comparative analysis, we found that the DO-CK model had the highest and most stable R<sup>2</sup>, consistent with the performance of the RMSE and MBE. Therefore, the DO-CK model is the optimal model for estimating DLR<sub>0</sub> over the Tibetan Plateau.

To explore the reasons for the differences in the accuracy of each model, we further compare all the models from the theoretical perspective. We find that only DO-CK directly considers the effect of T<sub>a</sub> and precipitable water on DLR. In the SW-CK model, only T<sub>a</sub> is considered, but the influence of e on DLR is not considered. The other five models are based on DLR calculated by Stefan-Boltzmann’s law; thus, the E<sub>s</sub> needs to be estimated by T<sub>a</sub> and e; e also needs to be estimated by the model. Thus, the entire estimation process would produce a certain amount of error accumulation, and the estimation accuracy of these five models is also relatively lower. In general, the DO-CK model has the best performance on the Tibetan Plateau. It should be noted that its performance elsewhere needs to be tested further.

The mean MBE of these seven clear-sky models is  $1.45 \text{ W/m}^2$  for AL,  $10.8 \text{ W/m}^2$  for AN,  $16.4 \text{ W/m}^2$  for TD,  $21.2 \text{ W/m}^2$  for BJ,  $38.4 \text{ W/m}^2$  for DX,  $15.2 \text{ W/m}^2$  for GZ,  $3.7 \text{ W/m}^2$  for HB,  $0.58 \text{ W/m}^2$  for MQ, and  $4.38 \text{ W/m}^2$  for NQ. These models had no fixed systematic errors in AL, HB, and MQ, but there are systematic overestimations or underestimations at the other sites. Further examinations reveal that all the models perform slightly better

for AL than for the other sites, as presented in Table 4. The reason for this phenomenon is that AL has different geographical and climatic backgrounds compared to the other sites. As demonstrated in Figure 1, AL is located on the southwestern edge of the Tibetan Plateau. It belongs to the monsoon climate zone and the subtropical mountain climate. The other sites on the Tibetan Plateau are located in the northwestern or northern part of the Tibetan Plateau, where the atmosphere is dry and clean, and the climate belongs to the plateau climate region. However, these models are all empirical models and have not been investigated in the plateau climate region. The atmospheric conditions and climatic conditions of AL are more similar to the study areas of these models, leading to this result.

Through our previous analysis of the various validation indices for  $\text{DLR}_0$  estimation results, it is clear that the DO-CK model is the most suitable model for estimating DLR under clear-sky conditions over the Tibetan Plateau. To further understand the performance of DO-CK, its estimates of  $\text{DLR}_0$  are further examined. The scatter plots of the ground-measured  $\text{DLR}_0$  and the estimated  $\text{DLR}_0$  based on the DO-CK model are provided in Figure 2; the MBE, RSME, and  $R^2$  values are also presented. According to the MBE values for the nine sites, it is evident that the DO-CK model has slight systematic deviations for all sites except DX and NQ. There is a certain overestimation for the DX site ( $\text{MBE} = 29.7 \text{ W/m}^2$ ), and an underestimation for the NQ site ( $\text{MBE} = -20.8 \text{ W/m}^2$ ). This finding reveals that the DO-CK model has no general positive/negative systematic errors over the Tibet Plateau. Nevertheless, we can see that some DLR samples are underestimated. The reason for the small undervaluation is mainly the misjudgment of the clear-sky conditions (i.e., the weather of a site is considered clear-sky when it is cloudy). This phenomenon suggests that DLR under cloudy conditions cannot be well estimated through this model.  $R^2$  ranging from 0.71 to 0.91 at the nine sites indicate that the estimated DLR has a good correlation with the measured DLR of the site. RMSE ranging from  $14.1 \text{ W/m}^2$  (AL) to  $34.3 \text{ W/m}^2$  (NQ) at the 9 sites indicate that the estimated DLR has acceptable accuracy.

The daytime mean  $T_a$  and  $e$  of the nine ground sites under clear-sky conditions are provided in Table 5.  $T_a$  and  $e$  are the main parameters in the DO-CK model; thus, it is necessary to test the sensitivity of the DO-CK model to these two parameters. From Table 5, it can be observed that the AL site has higher temperatures and humidity than the other eight sites.  $T_a$  fluctuation of the AL site is the lowest, and the fluctuation of water vapor pressure estimated from  $T_a$  is also lower than the other eight sites. This indicates that the atmospheric condition of AL is relatively stable. This finding supports our analysis of the reasons why all the models perform slightly better at AL than at the other sites. Thus, we divide the nine sites into two categories according to the daytime mean and standard deviation of  $T_a$ , each with a sensibility test. The first category is represented by the AL site. Its daytime  $T_a$  is  $286.7 \pm 3.5 \text{ K}$ . We test the sensitivity of  $e$  under three  $T_a$  conditions (i.e.,  $T_a = 286.7 - 3.5 \text{ K}$ ,  $T_a = 286.7 \text{ K}$ , and  $T_a = 286.7 + 3.5 \text{ K}$ ), and the test result is displayed in Figure 3a. Under these three  $T_a$  conditions, the effect of  $e$  on DLR is about  $4.0 \text{ W/hpa}$ . In the first category, the daytime mean  $e$  value is  $11.166 \pm 3.685 \text{ hpa}$ . Thus, we test the sensitivity of  $T_a$  under three  $e$  conditions (i.e.,  $e = 11.166 - 3.685 \text{ hpa}$ ,  $e = 11.166 \text{ hpa}$ , and  $e = 11.166 + 3.685 \text{ hpa}$ ), and the test result is provided in Figure 3b. Under these three  $e$  conditions, the effect of  $T_a$  on DLR is about  $2.4 \text{ W/K}$ . The sensitivity analysis results demonstrate that  $T_a$  and  $e$  can induce some estimation error to the DO-CK model. Thus, in addition to the error of the model itself, the error of the DO-CK model estimation result also contains the error caused by the input parameter error.

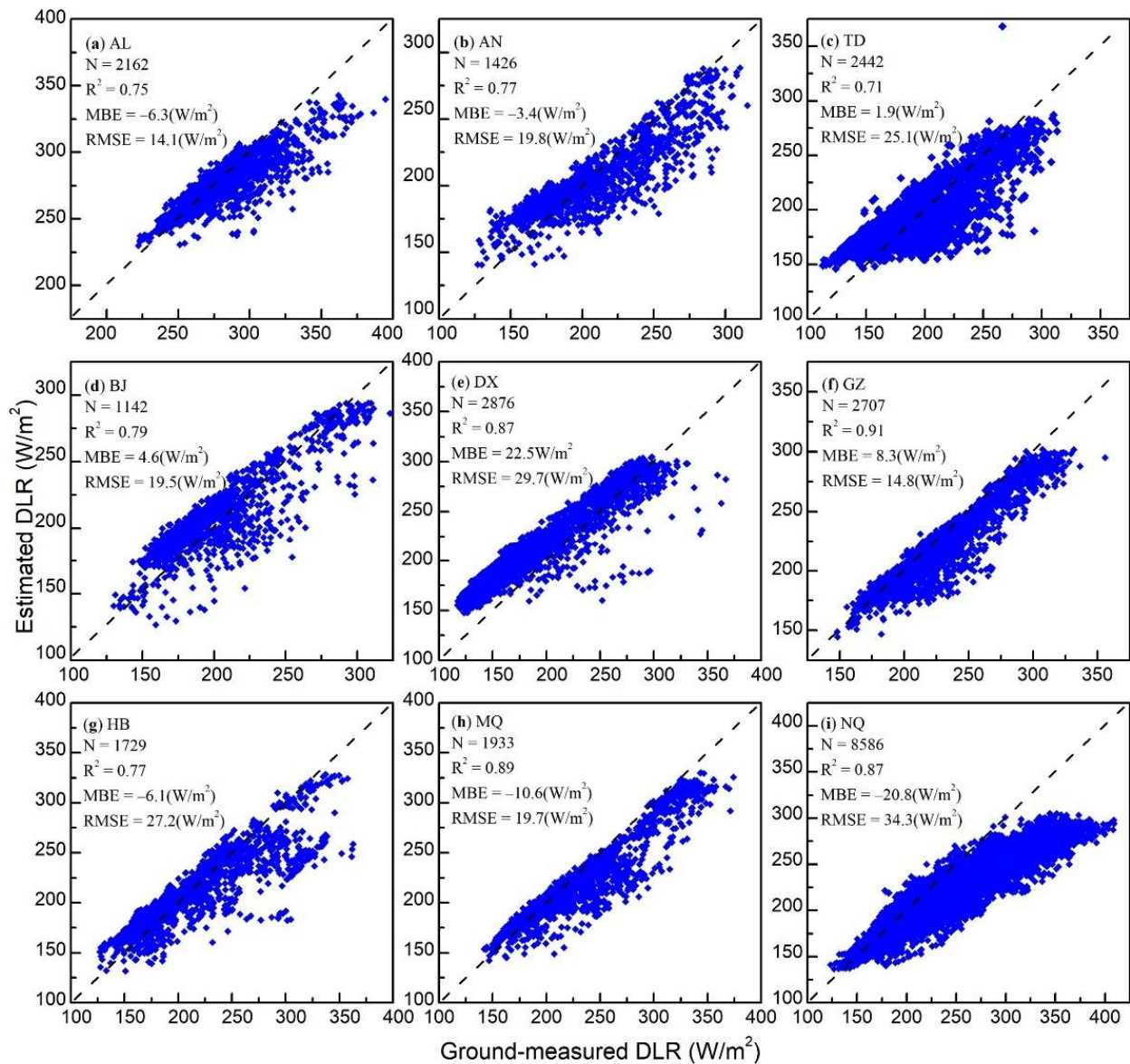


**Figure 2.** Scatter plots between the ground-measured and estimated DLR, based on the Dilly and O’Brien [9] (DO-CK) model, for the nine sites. N is the sample size. (a): AL site; (b): AN site; (c): TD site; (d): BJ site; (e): DX site; (f): GZ site; (g): HB site; (h): MQ site; (i): NQ site.

**Table 5.** The daytime mean and standard deviation of  $T_a$  and  $e$  for the nine ground sites under clear-sky conditions.

Site	Daytime Mean $T_a$ (K)	STD of $T_a$ (K)	Daytime Mean $e$ (hpa)	STD of $e$ (hpa)
AL	286.7	3.5	11.166	3.685
AN	271.7	6.3	3.145	1.794
BJ	275.2	7.8	3.907	2.659
TD	271.3	6.4	3.211	2.106
DX	278.4	6.7	3.994	2.750
GZ	277.5	7.8	2.555	1.998
HB	275.6	7.5	4.706	2.753
MQ	278.5	7.3	5.602	3.342
NQ	278.0	7.1	3.553	2.223

The other eight sites are classified into the second category, and the second category has lower  $T_a$  and  $e$ . The mean  $T_a$  and  $e$  of the second category site were  $275.8 \pm 7.1$  K and  $3.834 \pm 2.453$  hpa, respectively. Similar to the first category, we also tested the sensitivity of  $e$  and  $T_a$  under three  $T_a$  conditions (i.e.,  $T_a = 275.8 - 7.1$  K,  $T_a = 275.8$  K, and  $T_a = 275.8 + 7.1$  K) and three  $e$  conditions (i.e.,  $e = 3.834 - 2.453$  hpa,  $e = 3.834$  hpa, and  $e = 3.834 + 2.453$  hpa), and the test result is presented in Figure 3c,d. For the second category, the effect of  $e$  on DLR is approximately 6 W/hpa, and the effect of  $T_a$  on DLR is approximately 2.2 W/K.

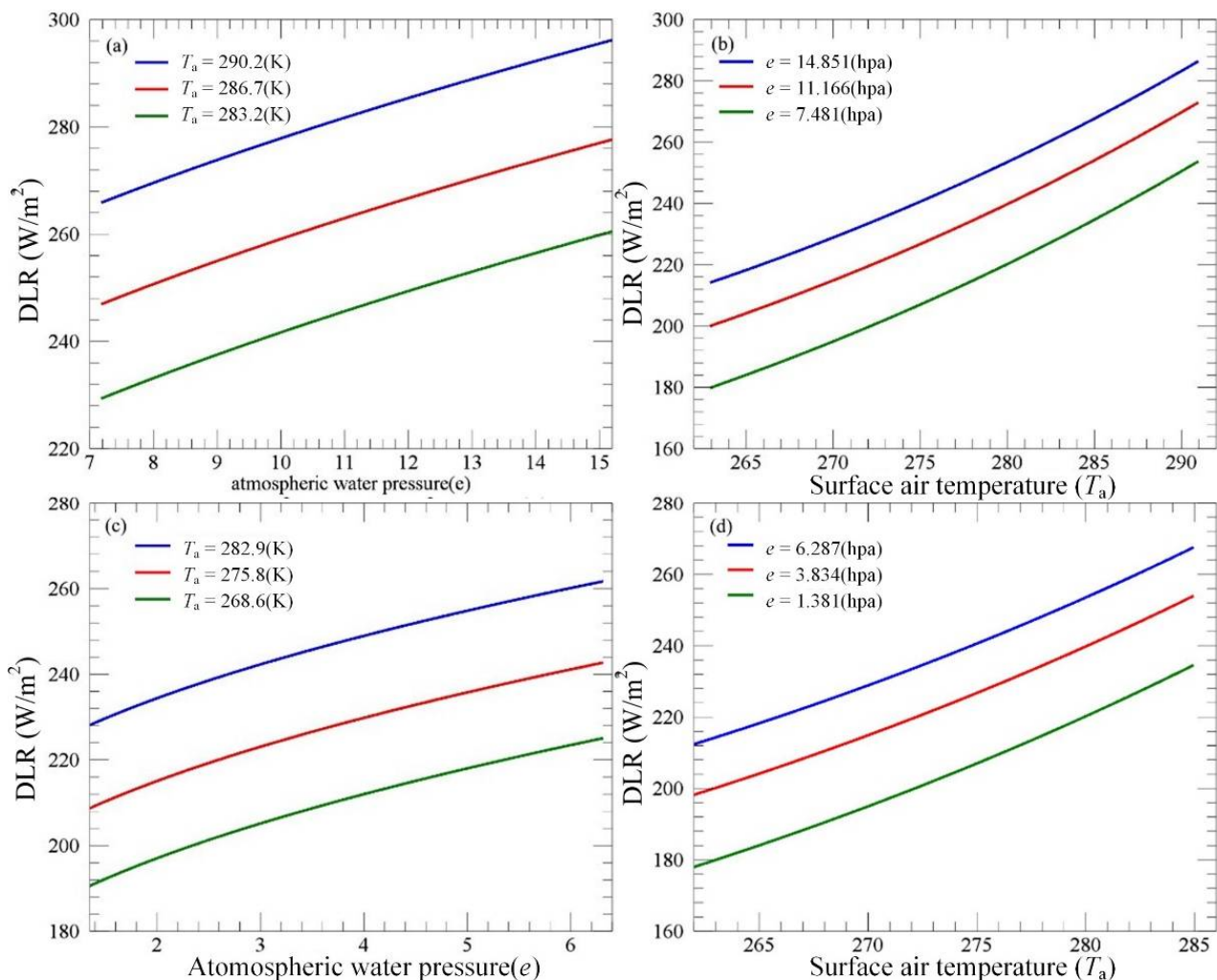


**Figure 3.** Sensitivity test results of DO-CK models for  $T_a$  and  $e$ . (a) the sensitivity of  $e$  under three  $T_a$  conditions for the AL site; (b) the sensitivity of  $T_a$  under three  $e$  conditions for the AL site; (c) the sensitivity of  $e$  under three  $T_a$  conditions for the other eight sites; (d) the sensitivity of  $T_a$  under three  $e$  conditions for the other eight sites.

#### 4.1.2. Under Cloudy Conditions

The estimation of DLR under cloudy conditions is necessary for obtaining the all-weather DLR. In this study, when  $c$  is higher than 0.05, the weather is assumed to be cloudy at the corresponding moment. Here,  $DLR_c$  at each site is estimated based on the models listed in Table 3. As described previously, these models are based on  $DLR_0$ , which is estimated with the DO-CK model. The atmospheric conditions in the different regions are different, and the appearance of clouds further exacerbates the complexity of the atmospheric conditions. To determine the most suitable model for estimating  $DLR_c$  over the Tibetan Plateau, the estimates of the six cloudy models are examined here.

RMSE values of the six cloud models as well as the DO-CK model are provided in Table 6. It is clear that if the effect of clouds on DLR under cloudy conditions is not

considered; even if the most suitable model (DO-CK) is used for estimating the local  $DLR_0$ , the estimation results still have large errors. In this study, the mean RMSE for the nine sites is  $44.9 \pm 8.6 \text{ W/m}^2$ , before considering the cloud coverage in the DO-CK model. When the six models for  $DLR_c$  are used, the estimation error is reduced. In particular, LH-CL has the smallest estimation error, with an average RMSE of  $23.2 \pm 3.1 \text{ W/m}^2$  for the nine sites.

To further quantify the systematic errors of the above six models, the MBE of the DO-CK model and the other six models of the estimation of  $DLR_c$  are calculated and are provided in Table 6. All six cloudy models have different systematic deviations, among which LH-CL has the smallest systematic deviation and the MBE is  $6.4 \pm 8.1 \text{ W/m}^2$ . According to the MBE values, we know that DO-CK does not consider the contribution of clouds to DLR. Thus, the estimate based on that model exhibits great underestimation. The six cloudy models alleviate the underestimation of DLR by DO-CK under cloudy conditions. There is minimal systematic error when LH-CL is used to estimate  $DLR_c$  over the Tibetan Plateau.

**Table 6.** Evaluation results of the estimated DLR under cloudy conditions by the six models as well as the DO-CK model, for the nine sites.

Method		Site									Average Value
		AL	AN	TD	BJ	DX	GZ	HB	MQ	NQ	
DO-CK (clear-sky model)	RMSE ( $\text{W/m}^2$ )	54.9	38.8	41.7	37.6	40.6	30.4	51.7	49.9	57.8	44.9
	MBE ( $\text{W/m}^2$ )	-48.4	-28.0	-25.7	-25.8	-25.4	-21.7	-43.1	-43.4	-52.3	-34.8
	R <sup>2</sup>	0.62	0.76	0.73	0.82	0.62	0.85	0.65	0.73	0.74	0.72
MC-CL	RMSE ( $\text{W/m}^2$ )	34.2	32.8	34.0	27.9	30.9	24.9	38.9	40.0	48.6	34.7
	MBE ( $\text{W/m}^2$ )	-28.5	-22.2	-17.6	-17.8	-16.9	-17.0	-31.0	-34.6	-42.6	-25.4
	R <sup>2</sup>	0.79	0.81	0.79	0.89	0.75	0.89	0.77	0.83	0.75	0.81
JA-CL	RMSE ( $\text{W/m}^2$ )	18.0	23.6	26.6	18.2	21.7	17.6	25.5	24.4	34.3	23.3
	MBE ( $\text{W/m}^2$ )	-5.8	-8.0	-2.6	-2.2	0.3	-3.6	-14.2	-17.6	-25.3	-8.8
	R <sup>2</sup>	0.82	0.83	0.81	0.91	0.82	0.89	0.82	0.88	0.76	-0.84
SB-CL	RMSE ( $\text{W/m}^2$ )	49.3	37.1	39.5	34.9	37.9	28.8	48.1	47.2	55.2	42.0
	MBE ( $\text{W/m}^2$ )	-43.5	-26.5	-23.6	-23.8	-23.2	-20.5	-40.1	-40.9	-49.9	-32.4
	R <sup>2</sup>	0.72	0.78	0.76	0.84	0.66	0.86	0.70	0.76	0.75	0.76
KO-CL	RMSE ( $\text{W/m}^2$ )	40.5	33.5	35.1	28.8	31.8	25.4	40.0	41.8	49.1	36.2
	MBE ( $\text{W/m}^2$ )	-34.1	22.5	-17.3	-18.5	-17.5	-17.4	-31.1	-36.3	-42.4	-21.3
	R <sup>2</sup>	0.74	0.80	0.76	0.88	0.74	0.89	0.74	0.81	0.72	0.79
CD-CL	RMSE ( $\text{W/m}^2$ )	21.1	25.0	31.3	22.0	28.1	22.4	23.1	18.1	29.6	24.5
	MBE ( $\text{W/m}^2$ )	-1.7	6.6	13.7	11.9	16.4	11.3	1.1	-6.6	-6.4	6.5
	R <sup>2</sup>	0.73	0.78	0.78	0.91	0.81	0.86	0.78	0.88	0.75	0.81
LH-CL	RMSE ( $\text{W/m}^2$ )	24.9	22.2	27.8	21.0	25.7	19.9	22.4	18.0	26.9	23.2
	MBE ( $\text{W/m}^2$ )	16.2	4.4	10.9	11.9	15.5	8.6	2.0	-2.2	-9.7	6.4
	R <sup>2</sup>	0.80	0.82	0.81	0.91	0.84	0.88	0.83	0.89	0.74	0.84

R<sup>2</sup> values between the estimated  $DLR_c$  and ground-measured DLR are also presented in Table 6. The average R<sup>2</sup> value is  $0.84 \pm 0.48$  for LH-CL. We can see that the estimation results based on LH-CL have the highest and most stable correlation with the ground-measured DLR. LH-CL could express approximately 84% of DLR under cloudy conditions. When we estimated  $DLR_c$  using the DO-CK model (clear-sky model), the R<sup>2</sup> value was only  $0.72 \pm 0.08$ .

Through the comparison of the six cloudy models, we find that MC-CL, JA-CL, and SB-CL have the same expression as LH-CL. In these four equations, the coefficient of  $c$  in LH-CL is the largest, and the coefficients of  $c$  in the other three equations are relatively smaller.  $c$  in MC-CL and SB-CL is added with a power higher than 1. Since  $c$  is lower than 1, the contribution of  $c$  to  $DLR_c$  is further reduced. MC-CL, JA-CL, and SB-CL do not fully express the contribution of clouds to DLR, which lead to the obvious underestimation of  $DLR_c$  by these three models. KO-CL and CD-CL have the same expression. When  $c$  is between 0 and 1, the fourth power of  $c$  is lower than  $c$ ; thus, KO-CL is weaker than CD-CL in describing the contribution of the cloud coverage to DLR. Therefore, KO-CL is

not very suitable for the Tibetan Plateau. As for CD-CL and LH-CL, the LH-CL model was developed to estimate DLR of the Andean Altiplano, which has similar altitude and atmospheric conditions to the Tibetan Plateau. Thus, LH-CL is most suitable for estimating  $DLR_c$  over the Tibetan Plateau. In addition, Table 3 also lists the study areas of the other five models, and we can see that there are some differences with the climatic conditions of the Tibetan Plateau, and it is difficult to have better applicability in the Tibetan Plateau. This conclusion is consistent with the evaluation results.

After a comprehensive analysis of the six estimation models, it is easy to understand that using DO-CK in combination with LH-CL can estimate DLR most accurately under cloudy conditions. We further analyze the performance of the LH-CL model at every site. The scatter plots between the ground-measured DLR and the estimates before considering the clouds by DO-CK, and the estimates after considering the clouds by LH-CL for the nine sites, are provided in Figure 4. Before considering the clouds, the MBE values range from  $-52.3 \text{ W/m}^2$  (NQ) to  $-21.7 \text{ W/m}^2$  (GZ), exhibiting a negative deviation of the estimated DLR by DO-CK. The corresponding RMSE values range from  $30.4 \text{ W/m}^2$  (GZ) to  $57.8 \text{ W/m}^2$  (NQ). After considering the cloud coverage, the MBE and RMSE values range from  $-9.7 \text{ W/m}^2$  (NQ) to  $16.2 \text{ W/m}^2$  (ALS), and  $-19.2 \text{ W/m}^2$  (GZ) to  $27.8 \text{ W/m}^2$  (TD). It is evident that LH-CL can be largely deficient in the negative deviation caused by DO-CK when clouds are present. The combination of LH-CL and DO-CK allows  $DLR_c$  to have an estimated error of less than  $30 \text{ W/m}^2$ .

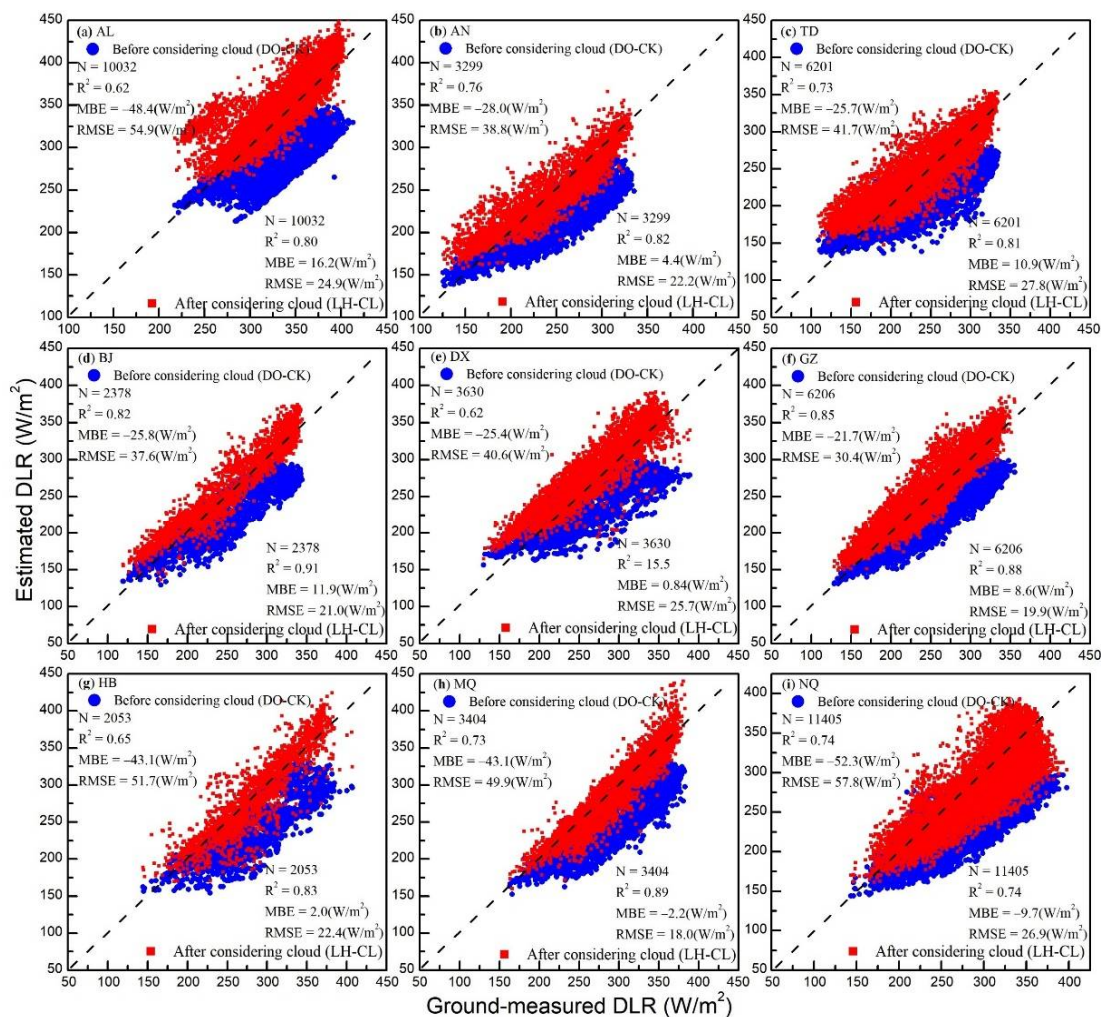


**Figure 4.** Evaluation results of DLR estimated by the Dillely and O'Brien [9] and Lhomme et al. [13] methods, based on the ground observation DLR at the nine sites. N is the sample size. (a): AL site; (b): AN site; (c): TD site; (d): BJ site; (e): DX site; (f): GZ site; (g): HB site; (h): MQ site; (i): NQ site.

#### 4.2. Estimated DLR for the Entire Tibetan Plateau, Based on the CLDAS Dataset

After comparing the models for estimating DLR under clear-sky and cloudy conditions, the DO-CK model is found to be suitable for clear-sky conditions, and the LH-CL model can be used to estimate  $DLR_c$  based on DO-CK for cloudy conditions.  $e$  in the DO-CK model can be calculated from  $p$ ,  $SH$ , and  $T_a$  derived from the CLDAS dataset according to Equation (4). Therefore, we can estimate the all-weather DLR over the entire Tibetan Plateau.

As mentioned previously, the time span of the CLDAS is from 2008 to 2016, and certain ground sites (i.e., AN, TD, BJ, and GZ) had no ground measurements during this period. Therefore, only five ground sites, including HB, NQ, AL, DX, and MQ, are used to evaluate the estimated all-weather DLR based on the CLDAS dataset. The evaluation results of the five sites are presented in Figure 5; MBE, RMSE, and  $R^2$  are also provided. To quantitatively evaluate the model that uses the ratio of DSR provided by the CLDAS to  $DSR_0$  to determine the cloud fraction, the all-weather DLR estimated directly by the DO-CK model is evaluated before considering the cloud coverage.

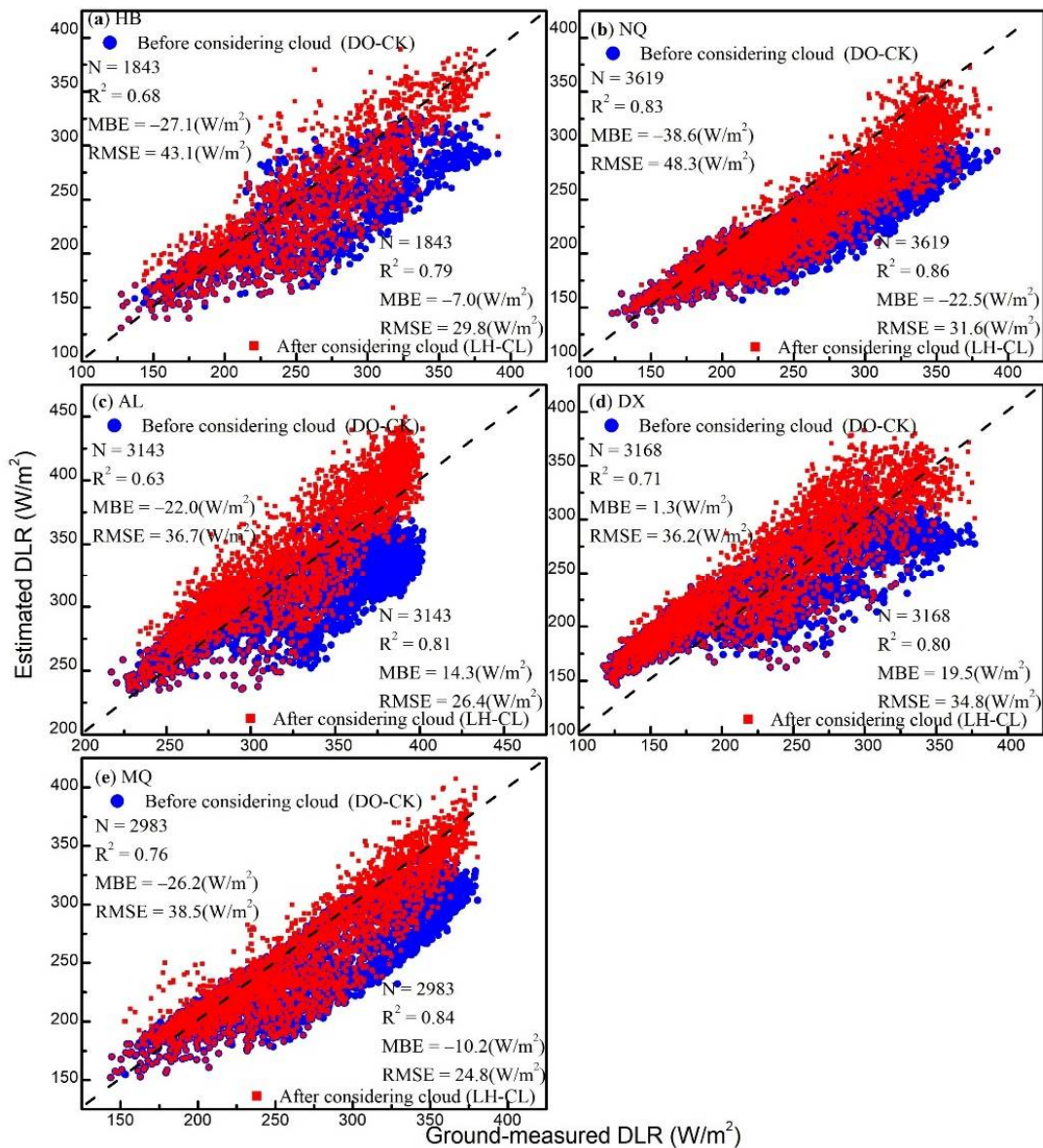


**Figure 5.** Scatter plots between the ground-measured DLR and the estimated DLR based on the CLDAS dataset at the five ground sites. N is the sample size. (a): HB; (b): NQ; (c): AL; (d): DX; (e): MQ.

Before considering the cloud coverage, the MBE and RMSE values of the DO-CK model range from  $-38.6$  to  $1.3 \text{ W/m}^2$  and  $36.2$  to  $48.3 \text{ W/m}^2$ , respectively. For HB, NQ, ALS, and MQ sites, the estimates of DLR yield large negative deviations. The main reason is that the presence of clouds increases the atmospheric moisture content and then increases DLR. However, the DO-CK model can only be applied under clear-sky conditions and does not take the contribution of clouds to DLR into account. For the DX site, although there is no significant negative deviation, a large error is still observed. The main reason is that DO-CK has a certain overestimation of DLR under clear-sky conditions for the DX site (as displayed in Figure 2e), which offset the underestimation under cloudy conditions and lead to no significant positive or negative deviation.

After considering the cloud coverage, the MBE and RMSE values range from  $-22.5$  to  $19.5 \text{ W/m}^2$  and  $24.9$  to  $34.8 \text{ W/m}^2$ , respectively. Compared with the results obtained without considering clouds, the LH-CL model can significantly reduce the underestimation of DLR by DO-CK. Specifically, for the HB, NQ, AL, and MQ sites, the negative deviations are decreased by approximately  $20 \text{ W/m}^2$ . The RMSE of all five sites is smaller than before considering the cloud coverage. The reduction in the RMSE ranges from  $1.4$  to  $16.7 \text{ W/m}^2$ . Therefore, the results demonstrate that the method based on the CLDAS dataset to account for clouds in the DSR determination is effective, and the estimated all-weather DLR of the Tibetan Plateau based on the CLDAS dataset has an acceptable accuracy.

To evaluate the contribution of the input parameters to the all-weather DLR estimation error, we calculate the error of  $T_a$  provided by CLDAS and  $e$  estimated based on CLDAS (Table 7). DLR estimation errors caused by  $T_a$  and  $e$  are also presented in Table 7. Note that the DLR estimation error mentioned here refers to the error in the all-weather DLR estimated by the DO-CK model before considering the influence of the cloud on DLR. From Table 7, it is clear that  $T_a$  and  $e$  have large estimation errors for the AL site, and their estimation errors caused a DLR estimation error of approximately  $20 \text{ W/m}^2$ . The influence of the cloud on instantaneous  $T_a$  and  $e$  is also very significant. Thus, cloud will increase the estimation error of  $T_a$  and  $e$ , and then the error of the estimated DLR becomes larger. After considering the influence of cloud on DLR, the estimation error of DLR is reduced by  $22.4 \text{ W/m}^2$  (Figure 5). The correction of  $\text{DLR}_c$  by the cloudy estimation model is actually to correct the DLR estimation error caused by the estimation error of  $T_a$  and  $e$ .  $T_a$  and  $e$  at the other four sites have different estimation errors, and DLR estimation errors induced by  $T_a$  and  $e$  are  $18.7 \text{ W/m}^2$  for MQ,  $13.4 \text{ W/m}^2$  for HB,  $11.5 \text{ W/m}^2$  for NQ, and  $93 \text{ W/m}^2$  for DX, respectively. After considering the influence of cloud on DLR through the LH-CL model, there is a significant positive correlation between the decrease of DLR estimation error at four sites and the estimation error caused by  $T_a$  and  $e$ . It can be observed that the error of the all-weather DLR estimation result is largely due to the uncertainty of the input parameters; the rest of the error is from the error of the model itself.

**Table 7.** Errors of  $T_a$  provided by CLDAS and  $e$  estimated based on CLDAS for five sites.

Site	$T_a$ RMSE (K)	DLR Error Caused by $T_a$ ( $\text{W/m}^2$ )	$e$ RMSE (hpa)	DLR Error Caused by $e$ ( $\text{W/m}^2$ )
AL	5.2	12.5	1.798	7.2
DX	1.4	3.1	1.032	6.2
HB	3.9	8.6	0.797	4.8
MQ	2.2	4.9	2.302	13.8
NQ	2.7	5.9	0.932	5.6

Note: the reference values are the ground measured values of  $T_a$  and  $e$  at the five sites.

To further understand the contribution of  $c$  estimated by the CLDAS to the estimation of the all-weather DLR, DOY 062 in 2012 is selected as an example, as many clouds appeared on this day. The spatial distributions of the values of  $c$  over the entire Tibetan Plateau during the daytime are provided in Figure 6. It can be observed that the cloud fraction over the Tibetan Plateau was low around sunrise (i.e., between 01:00 and 02:00 UTC) and sunset (i.e., at 09:00 UTC), whereas almost all the plateau was obscured by clouds at approximately noon (i.e., between 03:00–08:00 UTC). The value of  $c$  is larger in the southeastern part of the Tibetan Plateau but lower in the northwestern part. The main reason for this phenomenon

is that the air humidity in the southwestern part is more likely to form thick clouds; in contrast, the air humidity in the northwest part is lower, which is more likely to produce broken clouds [43,44].

The influences of the estimated  $c$  on the estimated DLR, based on the CLDAS data for the five ground sites, are further investigated (Figure 7). When the clouds are present, the estimated DLR would be significantly lower than the ground-measured DLR if the contribution of the clouds to DLR is not addressed. In contrast, after considering the contribution of the clouds, the estimated DLR has a much better agreement with the ground-measured DLR. In addition, the varying trend of the estimated DLR is basically consistent with the varying trend of the  $c$  values. The latter is especially true at the NQ and AL sites.

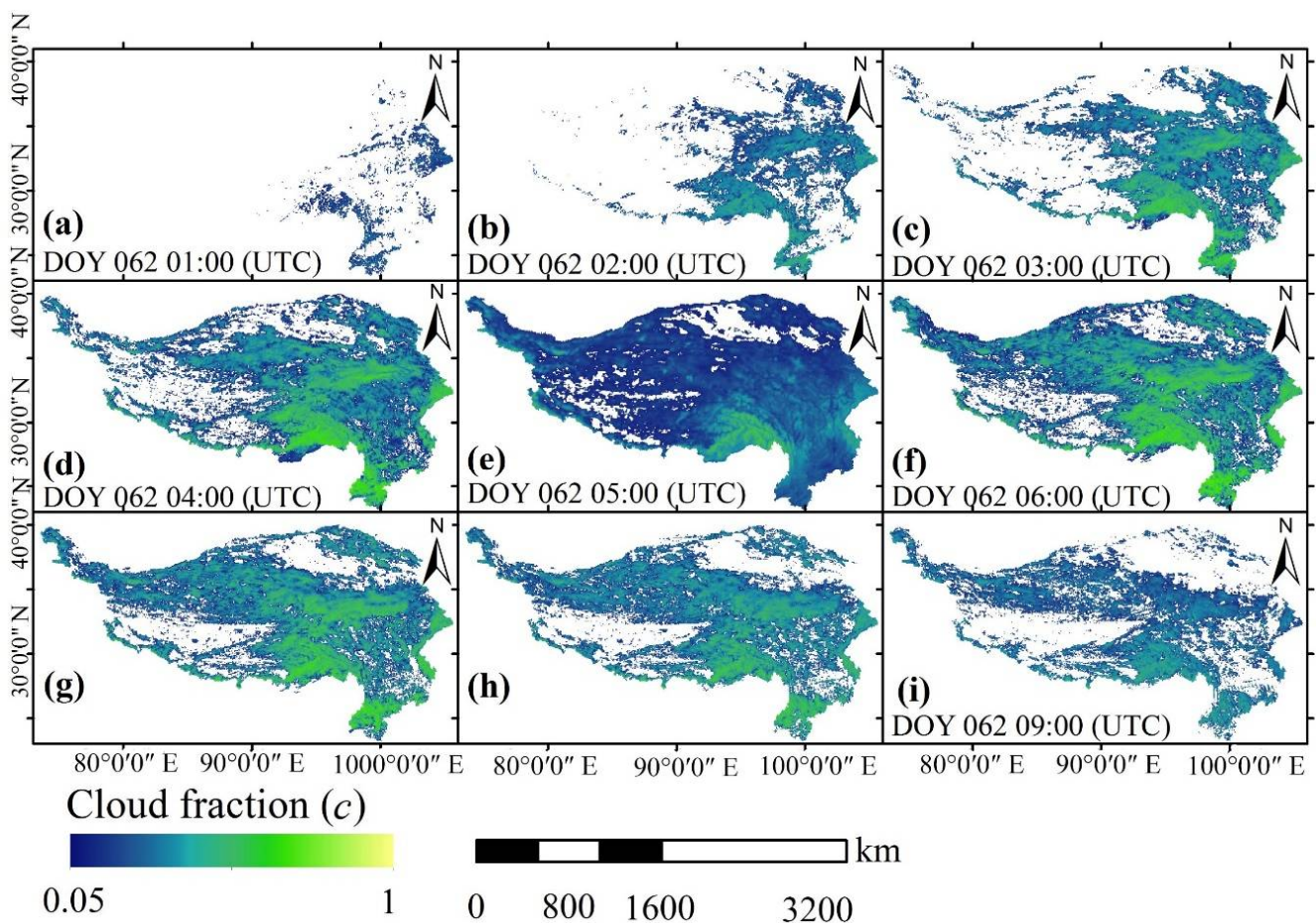


**Figure 6.** The spatial distribution of the cloud fraction over the entire Tibetan Plateau on DOY 062 in 2012. (a): DOY 062 01:00 (UTC); (b): DOY 062 02:00 (UTC); (c): DOY 062 03:00 (UTC); (d): DOY 062 04:00 (UTC); (e): DOY 062 05:00 (UTC); (f): DOY 062 06:00 (UTC); (g): DOY 062 07:00 (UTC); (h): DOY 062 08:00 (UTC); (i): DOY 062 09:00 (UTC).

Based on the aforementioned all-weather DLR models, we generate a DLR dataset with a  $0.0625^\circ$  spatial resolution and a 1-h temporal resolution for the entire Tibetan Plateau. The all-weather DLR at 06:00 UTC on DOY 001, 061, 122, 183, 245, and 305 in 2012 are presented in Figure 8 as examples. As displayed in Figure 1, the elevation of the southeastern Tibetan Plateau is low (approximately 60 to 4000 m); thus, the atmosphere in this region is humid and thick. In contrast, the average elevation is higher than 4000 m in the northwestern plateau, and the atmosphere is dry and thin. The difference in the atmosphere caused by the variation in elevation directly affected DLR. Therefore, we can clearly observe that DLR is higher in the southeast region of the Tibetan Plateau than in the northwest region. The temporal variations in DLR over the Tibetan Plateau are also very clear. DLR values displayed on DOY 122, 183, and 245 are significantly higher than DLR

values on DOY 001, 061, and 305. The main reason for this phenomenon is the variance in  $T_a$  in different seasons, as  $T_a$  is one of the main input parameters of the DRL model.

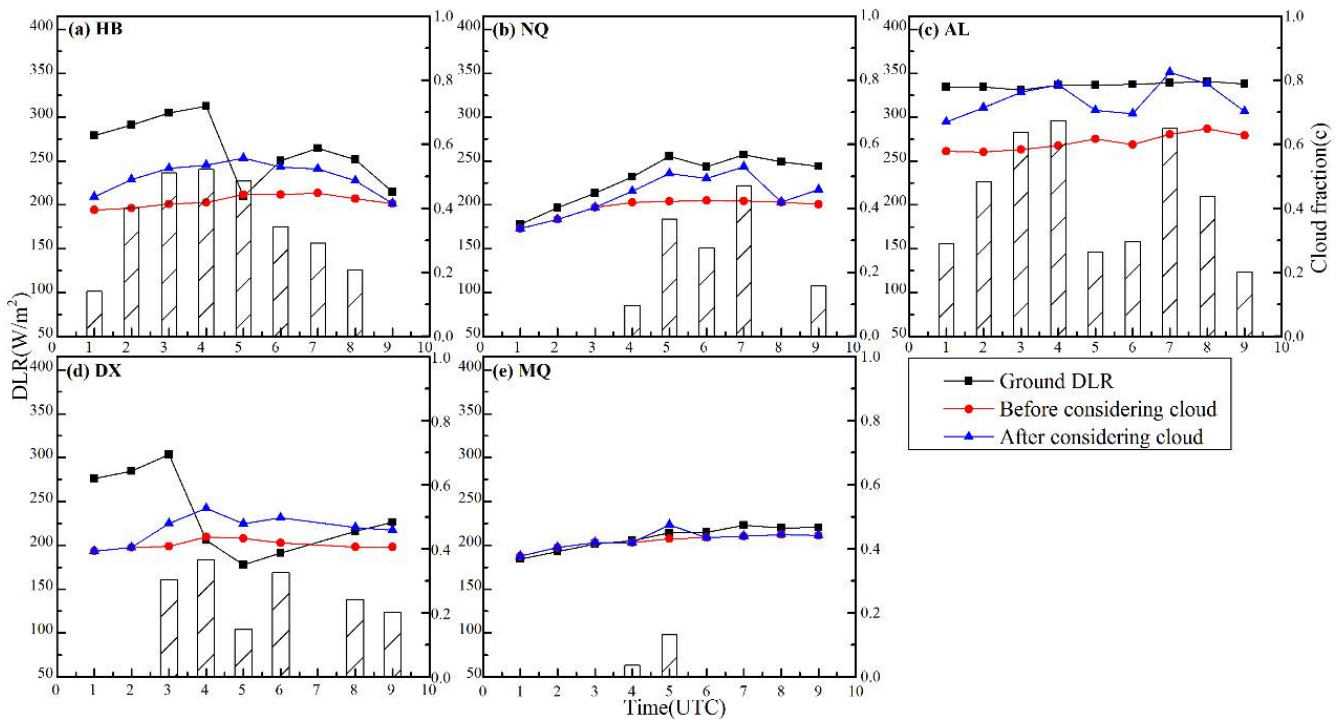


**Figure 7.** The ground-measured DLR, the estimated DLR before and after considering the cloud coverage, and the corresponding cloud fraction for the five ground sites on DOY 062 in 2012. (a): HB; (b): NQ; (c): AL; (d): DX; (e): MQ.

We further compare the all-weather DLR estimated based on CLDAS and the GLASS Longwave Radiation Product (GLASS-LRP) from the National Earth System Science Data Center, National Science & Technology Infrastructure of China (<http://www.geodata.cn>, accessed on 28 December 2020) [45]. Since GLASS-LRP is estimated based on MODIS observation data, its temporal resolution is daily, and its spatial resolution is 1 km. Its observation time is the MODIS overpassing time. In contrast, the temporal and spatial resolutions of the all-weather DLR are 1 h and 0.0625°, respectively. Therefore, it is difficult to accurately match these two data in the temporal and spatial dimensions. Here, these two DLR data are compared based on the RMSE obtained from this study and the developer of GLASS-LRP [45]. For GLASS-LRP, the average RMSE is 26.9 W/m<sup>2</sup>; for the all-weather DLR, the average RMSE is approximately 26.4 W/m<sup>2</sup> [45]. It is evident that the estimated all-weather DLR has a very similar accuracy to GLASS-LRP. On the one hand, the all-weather DLR estimated based on the CLDAS dataset has a higher temporal resolution and all-weather properties; on the other hand, GLASS-LRP has a much better spatial resolution.

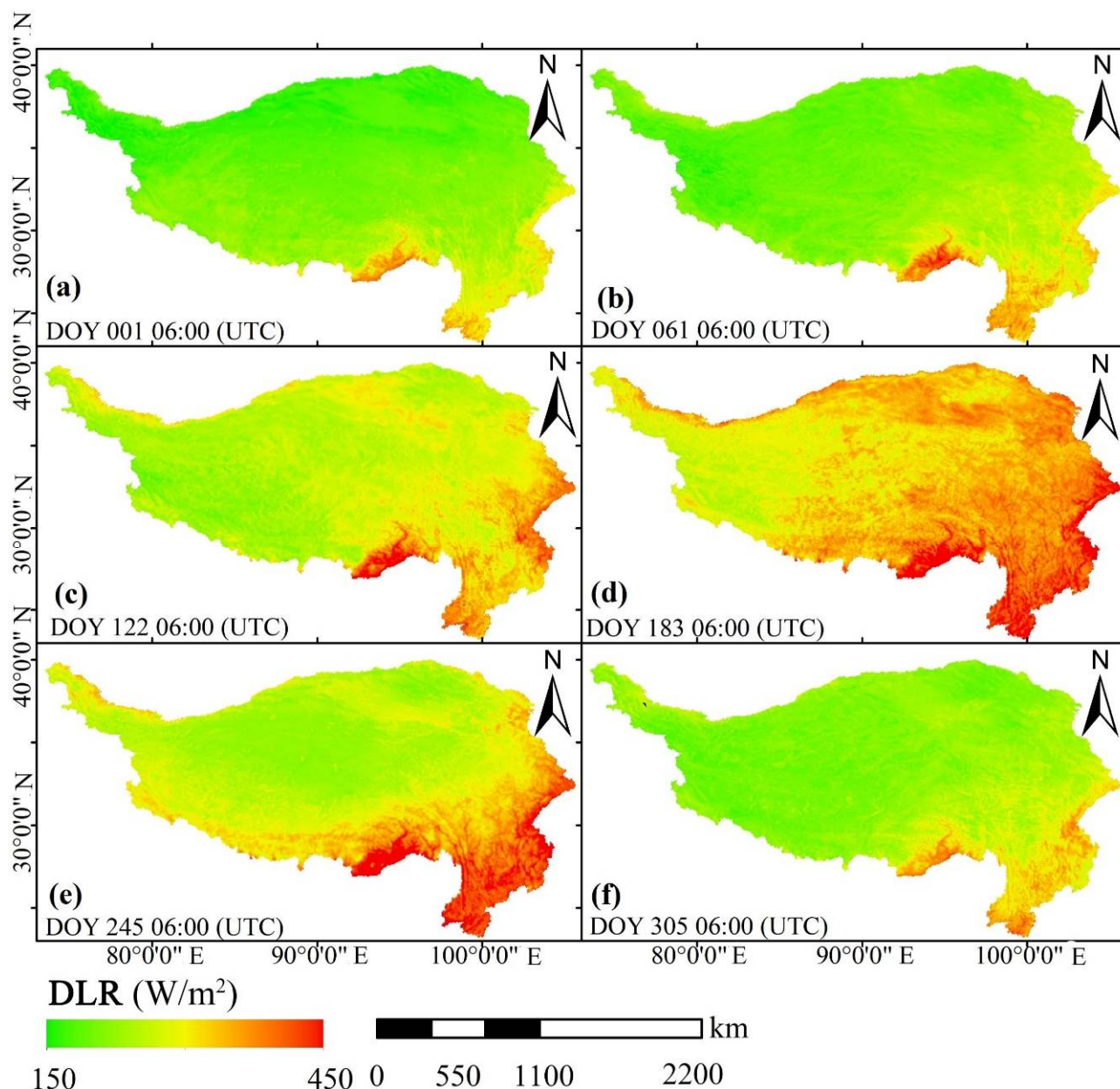


**Figure 8.** The estimated DLR, based on the CLDAS dataset over the entire Tibetan Plateau in 2012. (a): DOY 001 06:00 (UTC); (b): DOY 061 06:00 (UTC); (c): DOY 122 06:00 (UTC); (d): DOY 183 06:00 (UTC); (e): DOY 245 06:00 (UTC); (f): DOY 305 06:00 (UTC).

## 5. Conclusions

DLR is a critical parameter for radiation balance, energy budget, and water cycle studies at regional and global scales. In the past decades, there have been many studies on parameterization methods for estimating DLR. Based on these methods, several scientists have used satellite remote sensing data to estimate DLR. So far, most of DLR products that have been released involve instantaneous DLR products under clear-sky conditions. Therefore, the current DLR products that have a low temporal resolution and do not include the all-weather DLR are unable to meet the ever-increasing demands of related studies and applications. The Tibetan Plateau is a vital region for energy balance and climate change studies in Asia, even globally. Therefore, a high temporal resolution and the all-weather DLR are indispensable for related research on the Tibetan Plateau.

In this study, we compare eight models for estimating DLR under clear-sky conditions and six models for estimating DLR under cloudy conditions based on ground

measurements at nine spatially distributed sites located in the Tibetan Plateau. The results indicate that the models proposed by Dilley and O'Brien (1998) (i.e., the DO-CK model) and Lhomme et al. (2007) (i.e., the LH-CL model) are most suitable for clear-sky and cloudy conditions over the Tibetan Plateau, respectively. For DLR under clear-sky conditions, estimated by the DO-CK model, the mean RMSE is approximately  $22.5 \text{ W/m}^2$ . For DLR under cloudy conditions, estimated by the LH-CL model, the mean RMSE is approximately  $23.2 \text{ W/m}^2$ .

Based on the meteorological data provided by the CLDAS dataset, we further combine these two models to estimate the daytime all-weather DLR with a high temporal resolution (i.e., 1 h). Results demonstrate that the mean RMSE of the estimated DLR based on the CLDAS data is approximately  $26.4 \text{ W/m}^2$ , which represents an acceptable level of accuracy. Thus, estimating DLR based on assimilation data is a very effective way, and the parametric model is still one of the effective methods for estimating DLR. Meanwhile, based on the current study, the all-weather DLR with a 1 h temporal and  $0.0625^\circ$  spatial resolution for the entire Tibetan Plateau from 2008 to 2016 is generated. This DLR dataset will be beneficial to the long-term analysis of the radiation balance and energy budget over the Tibetan Plateau.

**Author Contributions:** Conceptualization, Z.L. and J.Z.; funding acquisition, J.Z.; investigation, L.D., Z.L. and T.Z.; methodology, Z.L. and L.D.; project administration, Z.L. All authors have read and agreed to the published version of the manuscript.

**Funding:** Ji Zhou was supported by the National Natural Science Foundation of China (grant number: 41871241 and 91647104), and by the Fundamental Research Funds for the Central Universities of China, University of Electronic Science and Technology of China (ZYGX2019J069).

**Informed Consent Statement:** Not applicable.

**Data Availability Statement:** All data needed to evaluate the conclusions made in this paper are included in the main body of the manuscript.

**Acknowledgments:** The China land surface data assimilation system (CLDAS) was provided by the China Meteorological Administration (CMA). The ground measurements were provided by the Coordinated Energy and Water Cycle Observation Project (CEOP), Enhanced Observing Periods 3 and 4 (EOP-3 and EOP-4), CEOP Asia-Australia Monsoon Project (CAMP), China FLUX Observation and Re-research Network, and the Northwest Institute of Eco-Environment and Resources of Chinese Academy of Sciences.

**Conflicts of Interest:** The authors declare no conflict of interest.

## Appendix A. The Calculation of $DSR_0$

In this study, the theoretical downward solar radiation ( $DSR_0$ ) in clear-sky is used as one of the main parameters of the cloud fraction.  $DSR_0$  is parameterized as [13,20]:

$$DSR_0 = R_{ex} \tau = R_{ex} \exp\left(\frac{-0.018q}{K_t \cos z}\right) \quad (A1)$$

where  $Z$  and  $K_t$  are the solar zenith angle and the turbidity coefficient ( $K_t = 1$  under clear-sky);  $q$  is the atmospheric pressure.

$q$  is calculated based on altitude  $h$  (in meters):

$$q(h) = 1013(1 - (0.0065h/293))^{5.26} \quad (A2)$$

$R_{ex}$  in Equation (A1) is parameterized as follows:

$$R_{ex} = I_0 d_T^2 \cos Z = I_0 d_T^2 (\sin \psi \sin \delta + \cos \psi \cos \delta \cos H) \quad (A3)$$

where  $I_0$  is the solar constant ( $1367 \text{ W/m}^2$ );  $d_r$  is the ratio of the mean sun-earth distance over the actual measure, depending on the day of the year ( $D$ );  $\psi$ ,  $\delta$ , and  $H$  are the latitude, solar declination, and hour angle, respectively.

The variables in Equation (A3) can be parameterized as follows:

$$d_r^2 = 1 + 0.33 \cos(2\pi D/365) \quad (\text{A4})$$

$$\delta = 0.409 \sin\left(\frac{2\pi D}{365} - 1.39\right) \quad (\text{A5})$$

$$H = \left(\frac{\pi}{12}\right)(12 - t_s) \quad (\text{A6})$$

$$t_s = t + L_c + S_c \quad (\text{A7})$$

where  $D$  and  $t_s$  (in hour) are the day of year (1–365 or 366) and local solar time, respectively;  $S_c$  is parameterized as follows:

$$S_c = 0.1645 \sin(2f) - 0.1255 \cos(f) + 0.0250 \sin(f) \quad (\text{A8})$$

$$f = \frac{2\pi(D - 81)}{364} \quad (\text{A9})$$

where  $t$ ,  $L_c$ , and  $S_c$  are the local time in hour, the correction for longitude in hour, and the seasonal correction for the solar time, respectively [13,20].

## References

1. Crawford, T.M.; Duchon, C.E. An Improved Parameterization for Estimating Effective Atmospheric Emissivity for Use in Calculating Daytime Downwelling Longwave Radiation. *J. Appl. Meteorol.* **1998**, *38*, 474–480. [CrossRef]
2. Duarte, H.F.; Dias, N.L.; Maggionto, S.R. Assessing Daytime Downward Longwave Radiation Estimates for Clear and Cloudy Skies in Southern Brazil. *Agric. For. Meteorol.* **2006**, *139*, 171–181. [CrossRef]
3. Ångström, A.K. *A Study of the Radiation of the Atmosphere: Based upon Observations of the Nocturnal Radiation during Expeditions to Algeria and to California*; Smithsonian Institution: Washington, DC, USA, 1915; Volume 65.
4. Brunt, D. Notes on Radiation in the Atmosphere. I. *Q. J. R. Meteorol. Soc.* **1932**, *58*, 389–420. [CrossRef]
5. Brutsaert, W. On a Derivable Formula for Long-wave Radiation from Clear Skies. *Water Resour. Res.* **1975**, *11*, 742–744. [CrossRef]
6. Idso, S.B. A Set of Equations for Full Spectrum and 8-to 14- $\mu\text{m}$  and 10.5-to 12.5- $\mu\text{m}$  Thermal Radiation from Cloudless Skies. *Water Resour. Res.* **1981**, *17*, 295–304. [CrossRef]
7. Idso, S.B.; Jackson, R.D. Thermal Radiation from the Atmosphere. *J. Geophys. Res.* **1969**, *74*, 5397–5403. [CrossRef]
8. Prata, A.J. A New Long-wave Formula for Estimating Downward Clear-sky Radiation at the Surface. *Q. J. R. Meteorol. Soc.* **1996**, *122*, 1127–1151. [CrossRef]
9. Dilley, A.C.; O'Brien, D.M. Estimating Downward Clear Sky Long-wave Irradiance at the Surface from Screen Temperature and Precipitable Water. *Q. J. R. Meteorol. Soc.* **1998**, *124*, 1391–1401. [CrossRef]
10. Swinbank, W.C. Long-wave Radiation from Clear Skies. *Q. J. R. Meteorol. Soc.* **1963**, *89*, 339–348. [CrossRef]
11. Jacobs, J.D. Radiation climate of broughton island. In *Energy Budget Studies in Relation to Fast-Ice Breakup Processes in Davis Strait*; University of Colorado, Institute of Arctic and Alpine Research: Boulder, CO, USA, 1978; pp. 105–120.
12. Konzelmann, T.; Wal, R.S.W.V.D.; Greuell, W.; Bintanja, R.; Henneken, E.A.C.; Abe-Ouchi, A. Parameterization of Global and Longwave Incoming Radiation for the Greenland Ice Sheet. *Glob. Planet. Chang.* **1994**, *9*, 143–164. [CrossRef]
13. Lhomme, J.P.; Vacher, J.J.; Rocheteau, A. Estimating Downward Long-Wave Radiation on the Andean Altiplano. *Agric. For. Meteorol.* **2007**, *145*, 139–148. [CrossRef]
14. Maykut, G.A.; Church, P.E. Radiation Climate of Barrow Alaska, 1962–1966. *J. Appl. Meteorol.* **1973**, *12*, 924–936. [CrossRef]
15. Sugita, M.; Brutsaert, W. Cloud Effect in the Estimation of Instantaneous Downward Longwave Radiation. *Water Resour. Res.* **1993**, *29*, 599–605. [CrossRef]
16. Choi, M.; Jacobs, J.M.; Kustas, W.P. Assessment of Clear and Cloudy Sky Parameterizations for Daily Downwelling Longwave Radiation over Different Land Surfaces in Florida, USA. *Geophys. Res. Lett.* **2008**, *35*, 288–299. [CrossRef]
17. Wang, K.; Liang, S. Global Atmospheric Downward Longwave Radiation over Land Surface under All-sky Conditions from 1973 to 2008. *J. Geophys. Res. Atmos.* **2009**, *114*. [CrossRef]
18. Carmona, F.; Rivas, R.; Caselles, V. Estimation of Daytime Downward Longwave Radiation under Clear and Cloudy Skies Conditions over a Sub-Humid Region. *Theor. Appl. Climatol.* **2014**, *115*, 281–295. [CrossRef]
19. Wang, W.; Liang, S. Estimation of High-Spatial Resolution Clear-Sky Longwave Downward and Net Radiation over Land Surfaces from MODIS Data. *Remote Sens. Environ.* **2009**, *113*, 745–754. [CrossRef]

20. Yu, S.; Xin, X.; Liu, Q.; Zhang, H. Estimation of Clear-Sky Downward Longwave Radiation from Satellite Data in Heihe River Basin of Northwest China. In Proceedings of the Geoscience and Remote Sensing Symposium, Vancouver, BC, Canada, 24–29 July 2011; pp. 269–272.
21. Wu, H.; Zhang, X.; Liang, S.; Yang, H.; Zhou, G. Estimation of Clear-sky Land Surface Longwave Radiation from MODIS Data Products by Merging Multiple Models. *J. Geophys. Res. Atmos.* **2012**, *117*. [[CrossRef](#)]
22. Yu, S.S.; Xin, X.Z.; Liu, Q.H. Estimation of Clear-Sky Longwave Downward Radiation from HJ-1B Thermal Data. *Sci. China* **2013**, *56*, 829–842. [[CrossRef](#)]
23. Wang, C.; Tang, B.H.; Wu, H.; Tang, R.; Li, Z.L. Estimation of Downwelling Surface Longwave Radiation under Heavy Dust Aerosol Sky. *Remote Sens.* **2017**, *9*, 207. [[CrossRef](#)]
24. Ding, L.; Zhou, J.; Zhang, X.; Liu, S.; Cao, R. Downscaling of Surface Air Temperature over the Tibetan Plateau Based on DEM. *Int. J. Appl. Earth Obs. Geoinf.* **2018**, *73*, 136–147. [[CrossRef](#)]
25. Zhang, X.; Zhou, J.; Liang, S.; Wang, D. A Practical Reanalysis Data and Thermal Infrared Remote Sensing Data Merging (RTM) Method for Reconstruction of a 1-Km All-Weather Land Surface Temperature. *Remote Sens. Environ.* **2021**, *260*, 112437. [[CrossRef](#)]
26. Joyce, R.J.; Janowiak, J.E.; Arkin, P.A.; Xie, P. CMORPH: A Method That Produces Global Precipitation Estimates from Passive Microwave and Infrared Data at High Spatial and Temporal Resolution. *J. Hydrometeorol.* **2004**, *5*, 487–503. [[CrossRef](#)]
27. Shi, C.X.; Xie, Z.H.; Hui, Q.; Liang, M.L.; Yang, X.C. China Land Soil Moisture EnKF Data Assimilation Based on Satellite Remote Sensing Data. *Sci. China Earth Sci.* **2011**, *54*, 1430–1440. [[CrossRef](#)]
28. Jia, B.; Xie, Z.; Dai, A.; Shi, C.; Chen, F. Evaluation of Satellite and Reanalysis Products of Downward Surface Solar Radiation over East Asia: Spatial and Seasonal Variations. *J. Geophys. Res. Atmos.* **2013**, *118*, 3431–3446. [[CrossRef](#)]
29. Wang, B.; Yaoming, M.A.; Weiqiang, M.A. Estimation of Land Surface Temperature Retrieved from EOS/MODIS in Naqu Area over Tibetan Plateau. *J. Remote Sens.* **2012**, *16*, 1289–1309.
30. Shi, P.-L.; Zhang, X.-Z.; Zhong, Z.-M.; Ouyang, H. Diurnal and Seasonal Variability of Soil CO<sub>2</sub> Efflux in a Cropland Ecosystem on the Tibetan Plateau. *Agric. For. Meteorol.* **2006**, *137*, 220–233. [[CrossRef](#)]
31. Zhang, X.; Shi, P.; Liu, Y.; Ouyang, H. Experimental Study on Soil CO<sub>2</sub> Emission in the Alpine Grassland Ecosystem on Tibetan Plateau. *Sci. China Ser. D* **2005**, *48*, 218–224.
32. Yu, L.; Wang, H.; Wang, G.; Song, W.; Huang, Y.; Li, S.-G.; Liang, N.; Tang, Y.; He, J.-S. A Comparison of Methane Emission Measurements Using Eddy Covariance and Manual and Automated Chamber-Based Techniques in Tibetan Plateau Alpine Wetland. *Environ. Pollut.* **2013**, *181*, 81–90. [[CrossRef](#)]
33. Shang, L.; Zhang, Y.; Lyu, S.; Wang, S. Seasonal and Inter-Annual Variations in Carbon Dioxide Exchange over an Alpine Grassland in the Eastern Qinghai-Tibetan Plateau. *PLoS ONE* **2016**, *11*, e0166837. [[CrossRef](#)]
34. Wen, J.; Lan, Y.; Su, Z.; Tian, H.; Shi, X.; Zhang, Y.; Wang, X. Advances in Observation and Modeling of Land Surface Processes Over the Source Region of the Yellow River. *Adv. Earth Sci.* **2011**, *26*, 575–586.
35. Zhang, Y.; Yu, G.; Yang, J.; Wimberly, M.C.; Zhang, X.; Tao, J.; Jiang, Y.; Zhu, J. Climate-Driven Global Changes in Carbon Use Efficiency. *Glob. Ecol. Biogeogr.* **2014**, *23*, 144–155. [[CrossRef](#)]
36. Uppala, S.M.; Dee, D.; Kobayashi, S.; Berrisford, P.; Simmons, A. Towards a Climate Data Assimilation System: Status Update of ERA-Interim. *ECMWF Newsl.* **2008**, *115*, 12–18.
37. Dee, D.P.; Uppala, S.M.; Simmons, A.J.; Berrisford, P.; Poli, P.; Kobayashi, S.; Andrae, U.; Balmaseda, M.A.; Balsamo, G.; Bauer, P. The ERA-Interim Reanalysis: Configuration and Performance of the Data Assimilation System. *Q. J. R. Meteorol. Soc.* **2011**, *137*, 553–597. [[CrossRef](#)]
38. Gao, L.; Bernhardt, M.; Schulz, K.; Chen, X. Elevation Correction of ERA-Interim Temperature Data in the Tibetan Plateau. *Int. J. Climatol.* **2017**, *37*, 3540–3552. [[CrossRef](#)]
39. Kalnay, E.; Kanamitsu, M.; Kistler, R.; Collins, W.; Deaven, D.; Gandin, L.; Iredell, M.; Saha, S.; White, G.; Woollen, J. The NCEP/NCAR 40-Year Reanalysis Project. *Bull. Am. Meteorol. Soc.* **1996**, *77*, 437–472. [[CrossRef](#)]
40. Onogi, K.; Tsutsui, J.; Koide, H.; Sakamoto, M.; Kobayashi, S.; Hatsushika, H.; Matsumoto, T.; Yamazaki, N.; Kamahori, H.; Takahashi, K. The JRA-25 Reanalysis. *J. Meteorol. Soc. Jpn.* **2007**, *85*, 369–432. [[CrossRef](#)]
41. Wang, S.; Zhang, M.; Sun, M.; Wang, B.; Huang, X.; Wang, Q.; Fang, F. Comparison of Surface Air Temperature Derived from NCEP/DOE R2, ERA-Interim, and Observations in the Arid Northwestern China: A Consideration of Altitude Errors. *Theor. Appl. Climatol.* **2015**, *119*, 99–111. [[CrossRef](#)]
42. Coulson, K.L. Characteristics of the Radiation Emerging from the Top of a Rayleigh Atmosphere—I: Intensity and Polarization. *Planet. Space Sci.* **1959**, *1*, 265–276. [[CrossRef](#)]
43. King, M.D.; Kaufman, Y.J.; Menzel, W.P.; Tanre, D. Remote Sensing of Cloud, Aerosol, and Water Vapor Properties from the Moderate Resolution Imaging Spectrometer (MODIS). *IEEE Trans. Geosci. Remote Sens.* **1992**, *30*, 2–27. [[CrossRef](#)]
44. King, M.D.; Menzel, W.P.; Kaufman, Y.J.; Tanré, D.; Gao, B.C.; Platnick, S.; Ackerman, S.A.; Remer, L.A.; Pincus, R.; Hubanks, P.A. Cloud and Aerosol Properties, Precipitable Water, and Profiles of Temperature and Water Vapor from MODIS. *IEEE Trans. Geosci. Remote Sens.* **2003**, *41*, 442–458. [[CrossRef](#)]
45. Cheng, J.; Liang, S.; Wang, W.; Guo, Y. An Efficient Hybrid Method for Estimating Clear-Sky Surface Downward Longwave Radiation from MODIS Data. *J. Geophys. Res. Atmos.* **2017**, *122*, 2616–2630. [[CrossRef](#)]